

Search for $B_s^0 \rightarrow \eta' X_{s\bar{s}}$ at Belle Using a Semi-Inclusive Method

S. Dubey,¹⁴ T. E. Browder,¹⁴ H. Aihara,⁸² S. Al Said,^{75,34} D. M. Asner,³ T. Aushev,¹⁷ R. Ayad,⁷⁵ V. Babu,⁸ S. Bahinipati,²⁰ P. Behera,²³ J. Bennett,⁴⁹ M. Bessner,¹⁴ B. Bhuyan,²¹ S. Bilokin,⁴³ J. Biswal,³⁰ A. Bobrov,^{4,59} G. Bonvicini,⁸⁶ A. Bozek,⁵⁶ M. Bračko,^{46,30} M. Campajola,^{27,52} D. Červenkov,⁵ B. G. Cheon,¹³ K. Chilikin,⁴⁰ H. E. Cho,¹³ K. Cho,³⁶ Y. Choi,⁷³ S. Choudhury,²² D. Cinabro,⁸⁶ S. Cunliffe,⁸ S. Das,⁴⁵ R. Dhamija,²² F. Di Capua,^{27,52} Z. Doležal,⁵ D. Dossett,⁴⁸ S. Eidelman,^{4,59,40} D. Epifanov,^{4,59} T. Ferber,⁸ B. G. Fulsom,⁶¹ R. Garg,⁶² V. Gaur,⁸⁵ N. Gabyshev,^{4,59} A. Garmash,^{4,59} A. Giri,²² P. Goldenzweig,³¹ B. Golob,^{42,30} D. Greenwald,⁷⁷ Y. Guan,⁷ K. Gudkova,^{4,59} C. Hadjivasiliou,⁶¹ K. Hayasaka,⁵⁸ H. Hayashii,⁵³ M. T. Hedges,¹⁴ W.-S. Hou,⁵⁵ C.-L. Hsu,⁷⁴ K. Inami,⁵¹ A. Ishikawa,^{15,11} R. Itoh,^{15,11} M. Iwasaki,⁶⁰ Y. Iwasaki,¹⁵ E.-J. Jang,¹² Y. Jin,⁸² C. W. Joo,³² K. K. Joo,⁶ A. B. Kaliyar,⁷⁶ T. Kawasaki,³⁵ H. Kichimi,¹⁵ C. H. Kim,¹³ D. Y. Kim,⁷² S. H. Kim,⁶⁹ Y.-K. Kim,⁸⁸ T. D. Kimmel,⁸⁵ K. Kinoshita,⁷ S. Korpar,^{46,30} P. Križan,^{42,30} R. Kroeger,⁴⁹ P. Krokovny,^{4,59} T. Kuhr,⁴³ R. Kulasiri,³³ R. Kumar,⁶⁵ K. Kumara,⁸⁶ Y.-J. Kwon,⁸⁸ K. Lalwani,⁴⁵ J. S. Lange,¹⁰ S. C. Lee,³⁸ C. H. Li,⁴¹ J. Li,³⁸ L. K. Li,⁷ Y. B. Li,⁶³ L. Li Gioi,⁴⁷ J. Libby,²³ D. Liventsev,^{86,15} C. MacQueen,⁴⁸ M. Masuda,^{81,66} T. Matsuda,⁵⁰ M. Merola,^{27,52} F. Metzner,³¹ K. Miyabayashi,⁵³ R. Mizuk,^{40,17} G. B. Mohanty,⁷⁶ S. Mohanty,^{76,84} T. J. Moon,⁶⁹ M. Nakao,^{15,11} A. Natochii,¹⁴ L. Nayak,²² M. Nayak,⁷⁸ N. K. Nisar,³ S. Nishida,^{15,11} K. Nishimura,¹⁴ S. Ogawa,⁷⁹ H. Ono,^{57,58} Y. Onuki,⁸² P. Oskin,⁴⁰ G. Pakhlova,^{17,40} S. Pardi,²⁷ S.-H. Park,⁸⁸ T. K. Pedlar,⁴⁴ R. Pestotnik,³⁰ L. E. Piilonen,⁸⁵ T. Podobnik,^{42,30} E. Prencipe,¹⁸ M. T. Prim,³¹ A. Rostomyan,⁸ N. Rout,²³ G. Russo,⁵² D. Sahoo,⁷⁶ Y. Sakai,^{15,11} S. Sandilya,²² A. Sangal,⁷ L. Santelj,^{42,30} T. Sanuki,⁸⁰ V. Savinov,⁶⁴ G. Schnell,^{1,19} C. Schwanda,²⁵ Y. Seino,⁵⁸ K. Senyo,⁸⁷ M. E. Sevier,⁴⁸ M. Shapkin,²⁶ C. Sharma,⁴⁵ J.-G. Shiu,⁵⁵ B. Shwartz,^{4,59} E. Solovieva,⁴⁰ M. Starič,³⁰ Z. S. Stottler,⁸⁵ J. F. Strube,⁶¹ K. Sumisawa,^{15,11} M. Takizawa,^{70,16,67} U. Tamponi,²⁸ K. Tanida,²⁹ Y. Tao,⁹ F. Tenchini,⁸ K. Trabelsi,³⁹ M. Uchida,⁸³ Y. Unno,¹³ S. Uno,^{15,11} Y. Ushiroda,^{15,11} Y. Usov,^{4,59} S. E. Vahsen,¹⁴ R. Van Tonder,² G. Varner,¹⁴ C. H. Wang,⁵⁴ E. Wang,⁶⁴ P. Wang,²⁴ M. Watanabe,⁵⁸ S. Watanuki,³⁹ X. Xu,⁷¹ B. D. Yabsley,⁷⁴ W. Yan,⁶⁸ S. B. Yang,³⁷ H. Ye,⁸ J. H. Yin,³⁷ Z. P. Zhang,⁶⁸ V. Zhilich,^{4,59} and V. Zhukova⁴⁰

(The Belle Collaboration)

¹University of the Basque Country UPV/EHU, 48080 Bilbao

²University of Bonn, 53115 Bonn

³Brookhaven National Laboratory, Upton, New York 11973

⁴Budker Institute of Nuclear Physics SB RAS, Novosibirsk 630090

⁵Faculty of Mathematics and Physics, Charles University, 121 16 Prague

⁶Chonnam National University, Gwangju 61186

⁷University of Cincinnati, Cincinnati, Ohio 45221

⁸Deutsches Elektronen-Synchrotron, 22607 Hamburg

⁹University of Florida, Gainesville, Florida 32611

¹⁰Justus-Liebig-Universität Gießen, 35392 Gießen

¹¹SOKENDAI (The Graduate University for Advanced Studies), Hayama 240-0193

¹²Gyeongsang National University, Jinju 52828

¹³Department of Physics and Institute of Natural Sciences, Hanyang University, Seoul 04763

¹⁴University of Hawaii, Honolulu, Hawaii 96822

¹⁵High Energy Accelerator Research Organization (KEK), Tsukuba 305-0801

¹⁶J-PARC Branch, KEK Theory Center, High Energy Accelerator Research Organization (KEK), Tsukuba 305-0801

¹⁷Higher School of Economics (HSE), Moscow 101000

¹⁸Forschungszentrum Jülich, 52425 Jülich

¹⁹IKERBASQUE, Basque Foundation for Science, 48013 Bilbao

²⁰Indian Institute of Technology Bhubaneswar, Satya Nagar 751007

²¹Indian Institute of Technology Guwahati, Assam 781039

²²Indian Institute of Technology Hyderabad, Telangana 502285

²³Indian Institute of Technology Madras, Chennai 600036

²⁴Institute of High Energy Physics, Chinese Academy of Sciences, Beijing 100049

²⁵Institute of High Energy Physics, Vienna 1050

²⁶Institute for High Energy Physics, Protvino 142281

²⁷INFN - Sezione di Napoli, 80126 Napoli

²⁸INFN - Sezione di Torino, 10125 Torino

²⁹Advanced Science Research Center, Japan Atomic Energy Agency, Naka 319-1195

³⁰J. Stefan Institute, 1000 Ljubljana

³¹Institut für Experimentelle Teilchenphysik, Karlsruher Institut für Technologie, 76131 Karlsruhe

- ³²*Kavli Institute for the Physics and Mathematics of the Universe (WPI), University of Tokyo, Kashiwa 277-8583*
- ³³*Kennesaw State University, Kennesaw, Georgia 30144*
- ³⁴*Department of Physics, Faculty of Science, King Abdulaziz University, Jeddah 21589*
- ³⁵*Kitasato University, Sagami-hara 252-0373*
- ³⁶*Korea Institute of Science and Technology Information, Daejeon 34141*
- ³⁷*Korea University, Seoul 02841*
- ³⁸*Kyungpook National University, Daegu 41566*
- ³⁹*Université Paris-Saclay, CNRS/IN2P3, IJCLab, 91405 Orsay*
- ⁴⁰*P.N. Lebedev Physical Institute of the Russian Academy of Sciences, Moscow 119991*
- ⁴¹*Liaoning Normal University, Dalian 116029*
- ⁴²*Faculty of Mathematics and Physics, University of Ljubljana, 1000 Ljubljana*
- ⁴³*Ludwig Maximilians University, 80539 Munich*
- ⁴⁴*Luther College, Decorah, Iowa 52101*
- ⁴⁵*Malaviya National Institute of Technology Jaipur, Jaipur 302017*
- ⁴⁶*University of Maribor, 2000 Maribor*
- ⁴⁷*Max-Planck-Institut für Physik, 80805 München*
- ⁴⁸*School of Physics, University of Melbourne, Victoria 3010*
- ⁴⁹*University of Mississippi, University, Mississippi 38677*
- ⁵⁰*University of Miyazaki, Miyazaki 889-2192*
- ⁵¹*Graduate School of Science, Nagoya University, Nagoya 464-8602*
- ⁵²*Università di Napoli Federico II, 80126 Napoli*
- ⁵³*Nara Women's University, Nara 630-8506*
- ⁵⁴*National United University, Miao Li 36003*
- ⁵⁵*Department of Physics, National Taiwan University, Taipei 10617*
- ⁵⁶*H. Niewodniczanski Institute of Nuclear Physics, Krakow 31-342*
- ⁵⁷*Nippon Dental University, Niigata 951-8580*
- ⁵⁸*Niigata University, Niigata 950-2181*
- ⁵⁹*Novosibirsk State University, Novosibirsk 630090*
- ⁶⁰*Osaka City University, Osaka 558-8585*
- ⁶¹*Pacific Northwest National Laboratory, Richland, Washington 99352*
- ⁶²*Panjab University, Chandigarh 160014*
- ⁶³*Peking University, Beijing 100871*
- ⁶⁴*University of Pittsburgh, Pittsburgh, Pennsylvania 15260*
- ⁶⁵*Punjab Agricultural University, Ludhiana 141004*
- ⁶⁶*Research Center for Nuclear Physics, Osaka University, Osaka 567-0047*
- ⁶⁷*Meson Science Laboratory, Cluster for Pioneering Research, RIKEN, Saitama 351-0198*
- ⁶⁸*Department of Modern Physics and State Key Laboratory of Particle Detection and Electronics, University of Science and Technology of China, Hefei 230026*
- ⁶⁹*Seoul National University, Seoul 08826*
- ⁷⁰*Showa Pharmaceutical University, Tokyo 194-8543*
- ⁷¹*Soochow University, Suzhou 215006*
- ⁷²*Soongsil University, Seoul 06978*
- ⁷³*Sungkyunkwan University, Suwon 16419*
- ⁷⁴*School of Physics, University of Sydney, New South Wales 2006*
- ⁷⁵*Department of Physics, Faculty of Science, University of Tabuk, Tabuk 71451*
- ⁷⁶*Tata Institute of Fundamental Research, Mumbai 400005*
- ⁷⁷*Department of Physics, Technische Universität München, 85748 Garching*
- ⁷⁸*School of Physics and Astronomy, Tel Aviv University, Tel Aviv 69978*
- ⁷⁹*Toho University, Funabashi 274-8510*
- ⁸⁰*Department of Physics, Tohoku University, Sendai 980-8578*
- ⁸¹*Earthquake Research Institute, University of Tokyo, Tokyo 113-0032*
- ⁸²*Department of Physics, University of Tokyo, Tokyo 113-0033*
- ⁸³*Tokyo Institute of Technology, Tokyo 152-8550*
- ⁸⁴*Utkal University, Bhubaneswar 751004*
- ⁸⁵*Virginia Polytechnic Institute and State University, Blacksburg, Virginia 24061*
- ⁸⁶*Wayne State University, Detroit, Michigan 48202*
- ⁸⁷*Yamagata University, Yamagata 990-8560*
- ⁸⁸*Yonsei University, Seoul 03722*

(Dated: December 23, 2024)

We report the first search for the penguin-dominated process $B_s^0 \rightarrow \eta' X_{s\bar{s}}$ using a semi-inclusive method. A 121.4 fb^{-1} integrated luminosity $\Upsilon(5S)$ data set collected by the Belle experiment, at the KEKB asymmetric-energy e^+e^- collider, is used. We observe no statistically significant signal and including all uncertainties, we set a 90% confidence level upper limit on the partial branching fraction at 1.4×10^{-3} for $M(X_{s\bar{s}}) \leq 2.4 \text{ GeV}/c^2$.

The study of the decay of B mesons — bound states of a b antiquark and either a u , d , s , or c quark — has been fruitful for the interrogation of rare processes, elucidating the strong and weak interactions of the Standard Model (SM) of particle physics. According to the SM flavor-changing neutral currents are forbidden in B decays at leading-order, but may effectively occur at higher-order in so-called “penguin” processes [1].

The CLEO collaboration measured a larger than expected branching fraction (BF) for the charmless decay (decays whose primary decay products lack a charm quark) $B \rightarrow \eta' X_s$ as $\mathcal{B}(B \rightarrow \eta' X_s) = [4.6 \pm 1.1 \text{ (stat.)} \pm 0.4 \text{ (syst.)} \pm 0.5 \text{ (bkg.)}] \times 10^{-4}$, with $M(X_s) < 2.35 \text{ GeV}/c^2$, where the third uncertainty is due to the background subtraction [2, 3]. BaBar measured $\mathcal{B}(B \rightarrow \eta' X_s) = [3.9 \pm 0.8 \text{ (stat.)} \pm 0.5 \text{ (syst.)} \pm 0.8 \text{ (model)}] \times 10^{-4}$, for the same $M(X_s)$ requirement [4]. Belle previously measured the BF for the related process $B \rightarrow \eta X_s$ as $\mathcal{B}(B \rightarrow \eta X_s) = [26.1 \pm 3.0 \text{ (stat.)} \pm 2.1 \text{ (syst.)} \pm 4.0 \text{ (model)}] \times 10^{-5}$ [5]. While the η' meson itself is interesting [6] as its mass is higher than is expected from symmetry considerations, it is the unexpected BF enhancement seen in these measurements that has generated considerable interest. In Ref. [7], for example, the predicted BF for $B \rightarrow \eta' X$ is 1.3×10^{-4} . Explanations for this apparent enhancement focus on processes such as the $b \rightarrow sg$ transition, which is modified to an anomalous $b \rightarrow sg^*$ process, where $g^* \rightarrow g\eta'$, with the gluon coupling to the η' singlet [8–14]. Hence, glueball coupling may provide an explanation for these decays involving the η' .

Inclusive $b \rightarrow sg$ processes have not yet been investigated using the B_s^0 meson. In this letter we report the first search for the decay $B_s^0 \rightarrow \eta' X_{s\bar{s}}$ using a semi-inclusive method [15] with data collected at the $\Upsilon(5S)$ resonance by the Belle detector at the KEKB asymmetric-energy e^+e^- collider in Japan [16].

To lowest order, the amplitude for $B_s^0 \rightarrow \eta' X_{s\bar{s}}$ contains contributions from QCD penguin diagrams, the anomalous $g\eta'$ coupling, the tree-level color-suppressed $b \rightarrow u$ diagram, and the $b \rightarrow s(\gamma, Z)$ electroweak penguin diagrams, shown in Fig. 1 [17].

The Belle detector is a large-solid-angle magnetic spectrometer that consists of a silicon vertex detector (SVD), a 50-layer central drift chamber (CDC), an array of aerogel threshold Cherenkov counters (ACC), a barrel-like arrangement of time-of-flight scintillation counters (TOF), and an electromagnetic calorimeter comprised of CsI(Tl) crystals (ECL) located inside a superconducting solenoid coil that provides a 1.5 T magnetic field. An iron flux-return located outside of the coil is instrumented to de-

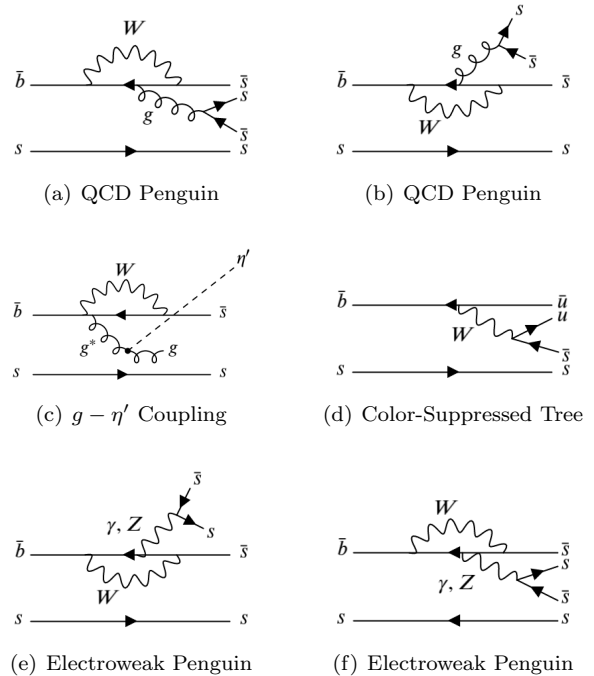


FIG. 1. Lowest-order diagrams contributing to $B_s^0 \rightarrow \eta' X_{s\bar{s}}$

tect K_L^0 mesons and to identify muons. The $\Upsilon(5S)$ data sample used a 1.5 cm radius beampipe, a 4-layer SVD, and a small-inner-cell CDC [18].

We use the 121.4 fb^{-1} data sample recorded by Belle, taken at the center-of-mass (CM) energy $\sqrt{s} = 10.866 \text{ GeV}$. This corresponds to $(7.11 \pm 1.30) \times 10^6 B_s^0 \bar{B}_s^0$ pairs, the world’s largest $\Upsilon(5S)$ sample in e^+e^- collisions [19]. A blind analysis is performed, whereby the selection criteria are first optimized on Monte Carlo (MC) simulations before being applied to the data. A signal MC sample for $B_s^0 \rightarrow \eta' X_{s\bar{s}}$ is generated using EvtGen [20] and the detector response is simulated using GEANT3 [21], with PHOTOS describing final-state radiation [22]. The MC-generated mass of the $X_{s\bar{s}}$ system is bounded below by the two-(charged) kaon mass $0.987 \text{ GeV}/c^2$ and has an upper bound of $3.0 \text{ GeV}/c^2$. The $X_{s\bar{s}}$ mass is generated as a flat distribution and is fragmented by PYTHIA 6 [23].

The B_s^0 ($\bar{b}s$) and \bar{B}_s^0 ($b\bar{s}$) candidates are reconstructed using a semi-inclusive method in which the $X_{s\bar{s}}$ is reconstructed as a system of two kaons, either K^+K^- or $K^\pm K_S^0 (\rightarrow \pi^+\pi^-)$, and up to four pions with at most one π^0 , where the π^0 decays via the channel $\pi^0 \rightarrow \gamma\gamma$. The η' is reconstructed in the channel $\eta' \rightarrow \eta (\rightarrow \gamma\gamma) \pi^+\pi^-$.

The experimental signature is divided into two classes of decay modes: without ($B_s^0 \rightarrow \eta' K^+ K^- + n\pi$) and with ($B_s^0 \rightarrow \eta' K^\pm K_S^0 + n\pi$) a K_S^0 . These classes are analyzed separately, with the weighted average BFs taken at the end. Charge-conjugate decays are included unless explicitly stated otherwise.

Well-constrained charged tracks are required to have a transverse momentum p_T greater than 50 MeV/ c . Separation of the charged kaons and charged pions is provided by the CDC [24], ACC [25], and the TOF [26] systems. Information from these subdetectors is combined to form a likelihood ratio for the charged kaon hypothesis: $P_{K^\pm} = L_{K^\pm}/(L_{K^\pm} + L_{\pi^\pm})$. For this analysis, the selections $P_{K^\pm} > 0.6$ for K^\pm and $P_{K^\pm} < 0.6$ for π^\pm are applied. The efficiency to correctly identify a pion (kaon) is 98% (88)%, with a misidentification rate of 4% (12)% [5].

The π^0 candidate mass range is $M(\gamma\gamma) \in [0.089, 0.180]$ GeV/ c^2 ($\pm 5\sigma$ window). The π^0 candidates are kinematically constrained to the nominal mass [27]. In the ECL, the photons constituting the π^0 are required to have energies greater than 50 MeV in the barrel region, greater than 100 MeV in the endcaps, and the ratio of their energy depositions in a 3×3 ECL crystal array to that in a 5×5 crystal array around the central crystal, is required to be greater than 0.9. To further reduce combinatorial background, a requirement on the π^0 laboratory-frame momentum to be greater than 0.2 GeV/ c is imposed.

The η is reconstructed in a two-photon asymmetric invariant mass window $M_\eta \in [0.476, 0.617]$ GeV/ c^2 ($5.3\sigma_L$, $10\sigma_R$). The asymmetry is due to energy leakage in the ECL, causing the η mass distribution to be asymmetric. Each photon is required to have $E_\gamma > 0.1$ GeV. A requirement on the photon-energy asymmetry ratio $|E_{\gamma 1} - E_{\gamma 2}|/(E_{\gamma 1} + E_{\gamma 2}) < 0.6$ is applied to further suppress the background. The η' mesons are reconstructed in a fully efficient mass window $M_{\eta'} \in [0.933, 0.982]$ GeV/ c^2 ($\pm 10\sigma$). The η and η' masses are kinematically fit to the world average [27]. The mass range of the K_S^0 is $M_{K_S^0} \in [0.487, 0.508]$ GeV/ c^2 ($\pm 3\sigma$ window).

The $X_{s\bar{s}}$ system is reconstructed as a system of kaons and pions, which is in turn combined with the η' to form B_s candidates. Two variables important in extracting the signal are the energy difference ΔE , defined as $\Delta E = E_{B_s} - E_{\text{beam}}$ and the beam-energy-constrained mass, defined as $M_{\text{bc}} = \sqrt{E_{\text{beam}}^2/c^4 - p_{B_s}^2/c^2}$, where $E_{\text{beam}} = \sqrt{s}/2$, E_{B_s} is the energy of the B_s , and p_{B_s} is the magnitude of the B_s three-momentum in the CM frame.

An initial reduction in continuum background ($e^+e^- \rightarrow q\bar{q}$, $q = u, d, s, c$) is done with a selection on the ratio of the second to the zeroth order Fox-Wolfram moments $R_2 \leq 0.6$ [28]. A neural network (NN), NeuroBayes [29], is used to further suppress continuum background, with other backgrounds being reduced as well. The NN is trained to primarily discriminate between event topolo-

gies using event shape variables [30]. Signal events have a spherical topology, while continuum background events are jet-like. The NN is trained using these variables on independent signal and continuum background MC simulations. The NN output variable O_{NN} describes, effectively, the probability that a B_s^0 candidate came from an event whose topology is spherical or jet-like.

To obtain a specific O_{NN} selection, the figure-of-merit (FOM) $S/\sqrt{S+B}$ is optimized as a function of O_{NN} , where S and B are the fitted signal and background yields from an MC sample that is passed through the trained network. This MC contains an approximately data-equivalent background and an enhanced signal. This was done assuming $\mathcal{B}(B_s^0 \rightarrow \eta' X_{s\bar{s}}) = 2 \times 10^{-4}$; this is 1.6 standard deviations below the BaBar central value for $B \rightarrow \eta' X_s$. The value of O_{NN} corresponding to the maximum value of the FOM is selected. Events having O_{NN} values below this selection are rejected. Separate optimizations are done for $B_s^0 \rightarrow \eta' K^+ K^- + n\pi$ and $B_s^0 \rightarrow \eta' K^\pm K_S^0 + n\pi$. The NN requirement reduces continuum background by more than 97% in both cases, while preserving 39% and 53% of signal events for $B_s^0 \rightarrow \eta' K^+ K^- + n\pi$ and $B_s^0 \rightarrow \eta' K^\pm K_S^0 + n\pi$, respectively. The two experimental signatures have different background levels and efficiencies, and hence their NNs are optimized separately.

After an initial requirement of $M_{\text{bc}} > 5.30$ GeV/ c^2 , $|\Delta E| < 0.35$ GeV, and $M(X_{s\bar{s}}) \leq 2.4$ GeV/ c^2 , and after all final selections are applied, there are an average of 6.4 candidates per event for $B_s^0 \rightarrow \eta' K^+ K^- + n\pi$ and 26.0 for $B_s^0 \rightarrow \eta' K^\pm K_S^0 + n\pi$. To select the best candidate per event, the candidate with the smallest χ^2 given by $\chi^2 = \chi_{\text{vtx}}^2/\text{ndf} + (\Delta E - \mu_{\Delta E})^2/\sigma_{\Delta E}^2$ is selected, where ΔE is calculated on a candidate-by-candidate basis, and $\mu_{\Delta E}$ is the mean energy difference obtained through studies of signal MC of individual exclusive $B_s^0 \rightarrow \eta' X_{s\bar{s}}$ decay modes. Here $\chi_{\text{vtx}}^2/\text{ndf}$ is the reduced χ^2 from a successful vertex fit of the primary charged daughter particles of the $X_{s\bar{s}}$. From signal MC, the efficiency of the best candidate selection is 85.5% for $B_s^0 \rightarrow \eta' K^+ K^- + n\pi$ and 43.2% for $B_s^0 \rightarrow \eta' K^\pm K_S^0 + n\pi$, in the signal region. The fraction of B_s^0 candidates passing best candidate selection that are correctly reconstructed is 94.0% for $B_s^0 \rightarrow \eta' K^+ K^- + n\pi$ and 60.4% for $B_s^0 \rightarrow \eta' K^\pm K_S^0 + n\pi$. These numbers are obtained after all final selections are applied.

Other backgrounds were studied as sources of potential peaking background. Due to the signal final state, it is difficult to have backgrounds that will be equivalent in topology and strangeness, and that are not highly suppressed. However, one such unmeasured mode is $B_s^0 \rightarrow \eta' D_s \pi$. Reconstruction efficiency is estimated using MC events and an expected number of peaking events is determined. For $B_s^0 \rightarrow \eta' D_s \pi$ the BF is assumed to be similar to $B^0 \rightarrow D^- \pi^+ \rho^0$, for which the world average is $[1.1 \pm 1.0] \times 10^{-3}$ [27]. After applying all final selections, the total number of expected peaking events is less than

one. There is a negligible amount of peaking background based on studies of $B_{(s)}^0 \bar{B}_{(s)}^0$ MC samples.

The decay $B \rightarrow \eta' K^{0*}$ can contribute to peaking background if the pion from $K^{0*} \rightarrow K^- \pi^+$ is misidentified. The world average BF is $[2.8 \pm 0.6] \times 10^{-6}$ [27]. From this and the pion misidentification rate, we expect the background contribution from this mode to be negligible.

The color-suppressed, tree-level process $B_s^0 \rightarrow \bar{D}^0 \eta'$, with $D^0 \rightarrow K^+ K^-$ could potentially contribute to the peaking background. However, $B^0 \rightarrow \bar{D}^0 \eta'$ has a measured BF of $\mathcal{B}(B^0 \rightarrow \bar{D}^0 \eta') = [1.38 \pm 0.16] \times 10^{-4}$. The process $D^0 \rightarrow K^+ K^-$ is Cabibbo-suppressed and has a measured BF of $\mathcal{B}(D^0 \rightarrow K^+ K^-) = [4.08 \pm 0.06] \times 10^{-3}$ [27]. Assuming $SU(3)$ symmetry, we expect there to be less than one event from $B_s^0 \rightarrow \bar{D}^0 \eta'$, for this analysis.

For signal extraction, fitting is done in $0.2 \text{ GeV}/c^2$ bins of $X_{s\bar{s}}$ mass, up to $2.4 \text{ GeV}/c^2$, using unbinned maximum-likelihood fits. All submodes are combined for fitting. Signal extraction is done by fitting the M_{bc} distribution in the region $M_{bc} > 5.30 \text{ GeV}/c^2$, $-0.12 \leq \Delta E \leq 0.05 \text{ GeV}$.

The $\Upsilon(5S)$ decays to B_s^0 pairs with a fraction of 0.172 ± 0.030 [19] and of this fraction the $\Upsilon(5S)$ has three channels for the B_s^0 decays: $\Upsilon(5S) \rightarrow B_s^{0*} \bar{B}_s^{0*}$, $\Upsilon(5S) \rightarrow B_s^0 \bar{B}_s^{0*}$ and $B_s^{0*} \bar{B}_s^0$, and $\Upsilon(5S) \rightarrow B_s^0 \bar{B}_s^0$. The rates are 87.0%, 7.3%, and 5.7%, respectively [19]. The low-energy photon from $B_s^{0*} \rightarrow B_s^0 \gamma$ is not reconstructed. This has the effect of shifting the mean of the ΔE distribution to a value of approximately -50 MeV .

The signal is modeled as the sum of three Gaussian probability density functions (PDFs) that correspond to the three $\Upsilon(5S)$ decays described in the previous paragraph. For analysis of the $\Upsilon(5S)$ data, their shape parameters are empirically derived from a $B_s^0 \rightarrow D_s^- \rho^+$ data control sample. The means and widths of the signal Gaussians are fixed from this. The dominant non-peaking background is from continuum with others coming from generic $B_s^{0(*)} \bar{B}_s^{0(*)}$ and $B\bar{B}X$ decays. The non-peaking background fit component is an ARGUS PDF [31] with a fixed shape parameter, determined from fits to $\Upsilon(5S)$ data NN sidebands. The ARGUS endpoint is fixed at $5.434 \text{ GeV}/c^2$, the kinematic limit of M_{bc} . The full model is the sum of the signal and background PDFs, with the signal and background yields allowed to float.

The signal reconstruction efficiency, defined as $\epsilon_i = N_i^{\text{rec}}/N_i^{\text{gen}}$, is determined from fitting signal MC sample, in each $X_{s\bar{s}}$ mass bin i after all selections are applied. Here, $N_i^{\text{gen}} = N_i^{B_s^0 \rightarrow \eta' K^+ K^- + n\pi} + N_i^{B_s^0 \rightarrow \eta' K^\pm K_S^0 + n\pi} + N_i^{\text{other}}$, is the number of generated B_s^0 mesons in the signal MC sample. The quantity N_i^{other} is the number of generated B_s^0 mesons that do not belong to either of the two classes of signal modes: $B_s^0 \rightarrow \eta' K^+ K^- + n\pi$ and $B_s^0 \rightarrow \eta' K^\pm K_S^0 + n\pi$ [32]. The quantity N_i^{rec} is the number of events found from the Gaussian signal fit in

the i -th $X_{s\bar{s}}$ mass bin.

The BF is calculated as $\mathcal{B}(B_s^0 \rightarrow \eta' X_{s\bar{s}})_i = N_i^{\text{sig}} / (2 \times N_{B_s^{0(*)} \bar{B}_s^{0(*)}}) \epsilon'_i [\mathcal{B}(\eta \rightarrow \gamma\gamma) \mathcal{B}(\eta' \rightarrow \pi^+ \pi^- \eta)]$, where i denotes the mass bins of $X_{s\bar{s}}$, the ϵ'_i are the bin-by-bin MC signal reconstruction efficiencies ϵ_i , corrected for data-MC discrepancies in NN selection, best candidate selection, particle identification, tracking efficiency, $\eta \rightarrow \gamma\gamma$ reconstruction, $\pi^0 \rightarrow \gamma\gamma$ reconstruction, and $K_S^0 \rightarrow \pi^+ \pi^-$ reconstruction. The quantity N_i^{sig} is the number of fitted signal events and the quantity $N_{B_s^{0(*)} \bar{B}_s^{0(*)}}$ is the number of produced $B_s^{0(*)} \bar{B}_s^{0(*)}$ pairs.

Figures 2 and 3 show the sum of the fits, whose results are listed in Tables I and II, respectively, overlaid on the data. The central value for $\mathcal{B}(B_s^0 \rightarrow \eta' X_{s\bar{s}})$ is estimated by taking the weighted average of the total BF central values for $B_s^0 \rightarrow \eta' K^+ K^- + n\pi$ and $B_s^0 \rightarrow \eta' K^\pm K^0 + n\pi$. These are obtained by summing the BFs listed in Tables I and II, for $B_s^0 \rightarrow \eta' K^+ K^- + n\pi$ and $B_s^0 \rightarrow \eta' K^\pm K^0 + n\pi$, respectively. The weights for the average central value are obtained from the statistical uncertainties. Systematic uncertainties are added in quadrature; fragmentation model (FM) uncertainties are added linearly within a class and for the final weighted average, these class sums are added in quadrature.

The statistical significance in each $X_{s\bar{s}}$ mass bin is calculated as $\mathcal{S} = \sqrt{-2 \ln(\mathcal{L}_0/\mathcal{L}_{\text{max}})}$, where \mathcal{L}_0 is the likelihood at zero signal yield and \mathcal{L}_{max} is the maximum likelihood. No statistically significant excess of events is observed in any $X_{s\bar{s}}$ mass bin. We set an upper limit on the partial BF (a BF with the requirement $M(X_{s\bar{s}}) \leq 2.4 \text{ GeV}/c^2$) at 90% confidence level by integrating a Gaussian likelihood function whose standard deviation is estimated by the sum in quadrature of the positive statistical and systematic uncertainties [33]. The standard deviation, σ , is approximately 8.6×10^{-4} . The integral is restricted to the physically allowed region above zero, giving an upper limit on $\mathcal{B}(B_s^0 \rightarrow \eta' X_{s\bar{s}})$. As a result, 1.68σ is added to the weighted average central value to obtain the 90% confidence level upper limit.

The central value of the BF is $\mathcal{B}(B_s^0 \rightarrow \eta' X_{s\bar{s}}) = [-0.7 \pm 8.1 \text{ (stat.)} \pm 0.7 \text{ (syst.)} \pm_{-6.0}^{+3.0} \text{ (FM)} \pm 0.1 \text{ (} N_{B_s^{0(*)} \bar{B}_s^{0(*)}} \text{)}] \times 10^{-4}$. The FM uncertainty is obtained by considering alternate sets of $X_{s\bar{s}}$ fragmentation parameter values in PYTHIA and redetermining the signal reconstruction efficiency [34].

The corresponding upper limit at 90% confidence level on the partial BF, including all uncertainties, is 1.4×10^{-3} for $M(X_{s\bar{s}}) \leq 2.4 \text{ GeV}/c^2$. If $SU(3)$ symmetry holds, then the BFs of $B \rightarrow \eta' X_s$ and $B_s^0 \rightarrow \eta' X_{s\bar{s}}$ would be equivalent and their ratio, $\mathcal{R}(\eta') = \mathcal{B}(B_s^0 \rightarrow \eta' X_{s\bar{s}})/\mathcal{B}(B \rightarrow \eta' X_s)$ would be close to 1 [17]. The measured BF for the decay $B \rightarrow \eta' X_s$ is $[3.9 \pm 0.8 \text{ (stat.)} \pm 0.5 \text{ (syst.)} \pm 0.8 \text{ (model)}] \times 10^{-4}$ [4]. Using this and the weighted average BF given previously for $B_s^0 \rightarrow \eta' X_{s\bar{s}}$, $\mathcal{R}(\eta')$ is approximately -0.2

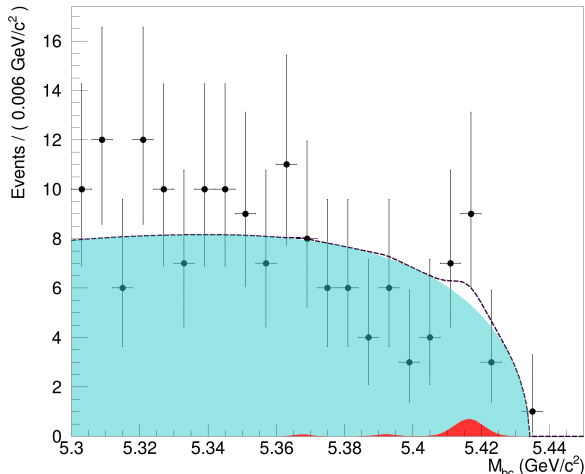


FIG. 2. Sum of the fits to all $M(X_{s\bar{s}})$ bins overlaid on the M_{bc} distribution, for the decay $B_s^0 \rightarrow \eta'(\rightarrow \eta\pi^+\pi^-)X_{s\bar{s}}$ for $B_s^0 \rightarrow \eta'K^+K^- + n\pi$ submodes and $M(X_{s\bar{s}}) \leq 2.4 \text{ GeV}/c^2$ and with all selections applied. The light blue shaded region is the sum of the background fits, the red shaded region is the sum of the signal fits, and the black dashed curve is the sum of the two.

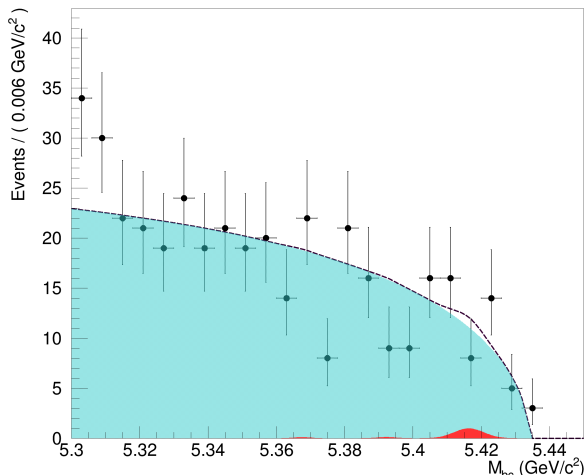


FIG. 3. Sum of the fits to all $M(X_{s\bar{s}})$ bins overlaid on the M_{bc} distribution, for the decay $B_s^0 \rightarrow \eta'(\rightarrow \eta\pi^+\pi^-)X_{s\bar{s}}$ for $B_s^0 \rightarrow \eta'K^\pm K_S^0 + n\pi$ submodes and $M(X_{s\bar{s}}) \leq 2.4 \text{ GeV}/c^2$ and with all selections applied. The light blue shaded region is the sum of the background fits, the red shaded region is the sum of the signal fits, and the black dashed curve is the sum of the two.

$\pm 2.1(\text{stat.}) \pm 0.2(\text{syst.})_{-1.5}^{+0.8}(\text{FM}) \pm 0.03(N_{B_s^{0(*)}}\bar{B}_s^{0(*)})$. Applying the same method as used to calculate the upper limit on $\mathcal{B}(B_s^0 \rightarrow \eta'X_{s\bar{s}})$, the 90% confidence level upper limit on $\mathcal{R}(\eta')$ is 3.5.

As a byproduct of the preceding measurement, we

TABLE I. Results for the $B_s^0 \rightarrow \eta'K^+K^- + n\pi$ submodes, from the $121.4 \text{ fb}^{-1} \Upsilon(5S)$ data set; the table contains the $M(X_{s\bar{s}})$ bin in units of GeV/c^2 , corrected reconstruction efficiency (ϵ'), number of fitted signal events N_{sig} , and \mathcal{B} , the central value of the partial BF.

$M(X_{s\bar{s}})$	ϵ' (%)	N_{sig}	$\mathcal{B}(B_s^0 \rightarrow \eta'X_{s\bar{s}}) (10^{-4})$
1.0 - 1.2	3.6 ± 0.08	$0.4_{-1.9}^{+2.6}$	$0.05_{-0.22}^{+0.30}$ (stat.) $_{-0.005}^{+0.004}$ (syst.)
1.2 - 1.4	2.8 ± 0.08	$0.08_{-1.7}^{+2.4}$	$0.01_{-0.28}^{+0.36}$ (stat.) $_{-0.001}^{+0.001}$ (syst.)
1.4 - 1.6	0.9 ± 0.04	$0.7_{-1.8}^{+2.5}$	$0.3_{-0.8}^{+1.1}$ (stat.) $_{-0.04}^{+0.04}$ (syst.)
1.6 - 1.8	0.5 ± 0.03	$0.4_{-1.4}^{+2.1}$	$0.3_{-1.1}^{+1.6}$ (stat.) $_{-0.1}^{+0.05}$ (syst.)
1.8 - 2.0	0.3 ± 0.03	$1.4_{-2.0}^{+2.6}$	$1.7_{-2.5}^{+3.3}$ (stat.) $_{-0.6}^{+0.4}$ (syst.)
2.0 - 2.2	0.2 ± 0.02	$0.3_{-3.4}^{+3.7}$	$0.6_{-6.4}^{+7.1}$ (stat.) $_{-0.2}^{+0.2}$ (syst.)
2.2 - 2.4	0.1 ± 0.02	$-2.3_{-3.4}^{+3.8}$	$-7.0_{-10.4}^{+11.6}$ (stat.) $_{-4.1}^{+1.7}$ (syst.)

TABLE II. Results for the $B_s^0 \rightarrow \eta'K^\pm K_S^0 + n\pi$ submodes, from the $121.4 \text{ fb}^{-1} \Upsilon(5S)$ data set; rows with dashes indicate bins where no events, background or signal, were found; the table contains the $M(X_{s\bar{s}})$ bin in units of GeV/c^2 , corrected reconstruction efficiency (ϵ'), number of fitted signal events N_{sig} , and \mathcal{B} , the central value of the partial BF.

$M(X_{s\bar{s}})$	ϵ' (%)	N_{sig}	$\mathcal{B}(B_s^0 \rightarrow \eta'X_{s\bar{s}}) (10^{-4})$
1.0 - 1.2	0.02 ± 0.006	0.0	-
1.2 - 1.4	0.2 ± 0.02	$0.3_{-0.8}^{+1.4}$	$0.5_{-1.5}^{+2.5}$ (stat.) $_{-0.04}^{+0.1}$ (syst.)
1.4 - 1.6	0.9 ± 0.04	$2.0_{-2.2}^{+3.0}$	$1.0_{-1.1}^{+1.4}$ (stat.) $_{-0.07}^{+0.1}$ (syst.)
1.6 - 1.8	0.6 ± 0.04	$1.2_{-2.6}^{+3.3}$	$0.8_{-1.6}^{+2.1}$ (stat.) $_{-0.1}^{+0.1}$ (syst.)
1.8 - 2.0	0.4 ± 0.03	$4.8_{-3.4}^{+4.2}$	$4.4_{-3.1}^{+3.9}$ (stat.) $_{-0.7}^{+0.9}$ (syst.)
2.0 - 2.2	0.4 ± 0.03	$-2.4_{-3.2}^{+3.9}$	$-2.8_{-3.8}^{+4.6}$ (stat.) $_{-0.7}^{+0.9}$ (syst.)
2.2 - 2.4	0.2 ± 0.02	$-1.1_{-2.9}^{+3.6}$	$-2.6_{-7.1}^{+8.9}$ (stat.) $_{-1.9}^{+0.2}$ (syst.)

searched for the decay $B_s^0 \rightarrow \eta'\phi$, with $\phi \rightarrow K^+K^-$. This decay was searched for in the $X_{s\bar{s}}$ mass subrange $M(X_{s\bar{s}}) \in [1.006, 1.03] \text{ GeV}/c^2$ ($\pm 3\sigma$ window). From MC simulations, the reconstruction efficiency is determined to be $7.90 \pm 0.03\%$. No statistically significant signal is found and the upper limit at 90% confidence level is determined to be 3.6×10^{-5} . The result from fitting is shown in Fig. 4. LHCb determines the upper limit at 90% confidence level to be 8.2×10^{-7} [35].

To conclude, we set an upper limit on the partial BF for the decay $B_s^0 \rightarrow \eta'X_{s\bar{s}}$, for $M(X_{s\bar{s}}) \leq 2.4 \text{ GeV}/c^2$. Including all uncertainties, the upper limit at 90% confidence level is determined to be 1.4×10^{-3} . This is the first result for the decay $B_s^0 \rightarrow \eta'X_{s\bar{s}}$. Future measurements may help elucidate $SU(3)$ symmetries and enhance the understanding of different penguin contributions to the amplitude of $b \rightarrow sg$ decays. This and future analyses should also help to motivate further studies, both experimental and theoretical, of inclusive B_s^0 processes as there is a dearth of research of the B_s^0 relative to B_d^0 and B_u^\pm .

We thank the KEKB group for excellent operation

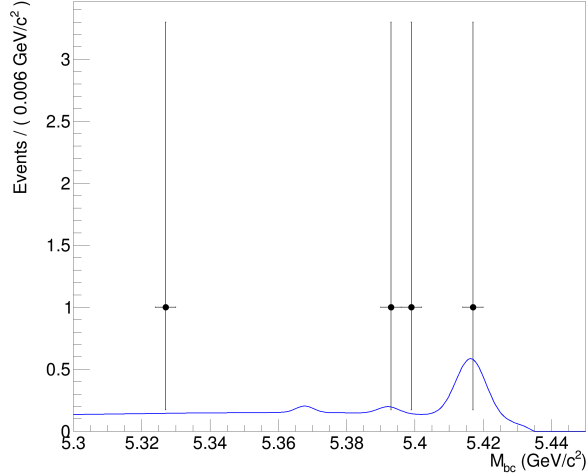


FIG. 4. $B_s^0 \rightarrow \phi(\rightarrow K^+ K^-) \eta'$ decay results for $M(X_{s\bar{s}}) \in \pm 3\sigma \phi$ mass range

of the accelerator; the KEK cryogenics group for efficient solenoid operations; and the KEK computer group, the NII, and PNNL/EMSL for valuable computing and SINET5 network support. We acknowledge support from MEXT, JSPS and Nagoya's TLPRC (Japan); ARC (Australia); FWF (Austria); NSFC and CCEPP (China); MSMT (Czechia); CZF, DFG, EXC153, and VS (Germany); DST (India); INFN (Italy); MOE, MSIP, NRF, RSRI, FLRFAS project, GSDC of KISTI and KREONET/GLORIAD (Korea); MNiSW and NCN (Poland); MSHE, Agreement 14.W03.31.0026 (Russia); University of Tabuk (Saudi Arabia); ARRS (Slovenia); IKERBASQUE (Spain); SNSF (Switzerland); MOE and MOST (Taiwan); and DOE and NSF (USA).

-
- [1] A. J. Bevan *et al.*, *Eur. Phys. J. C* **74**, 3026 (2014).
 [2] T. E. Browder *et al.* (CLEO Collaboration), *Phys. Rev. Lett.* **81**, 1786 (1998).
 [3] G. Bonvicini *et al.* (CLEO Collaboration), *Phys. Rev. D* **68**, 011101 (2003).
 [4] B. Aubert *et al.* (BABAR Collaboration), *Phys. Rev. Lett.* **93**, 061801 (2004).
 [5] K. Nishimura *et al.* (Belle Collaboration), *Phys. Rev. Lett.* **105**, 191803 (2010).

- [6] K. Ottnad and C. Urbach (ETM Collaboration), *Phys. Rev. D* **97**, 054508 (2018).
 [7] A. Datta, X.-G. He, and S. Pakvasa, *Phys. Lett. B* **419**, 369 (1998).
 [8] D. Atwood and A. Soni, *Phys. Lett. B* **405**, 150 (1997).
 [9] A. L. Kagan and A. Petrov, (1997), arXiv:hep-ph/9707354 [hep-ph].
 [10] H. Fritzsche, *Phys. Lett. B* **415**, 83 (1997).
 [11] W.-S. Hou and B. Tseng, *Phys. Rev. Lett.* **80**, 434 (1998).
 [12] A. Ali and A. Y. Parkhomenko, (2001), arXiv:hep-ph/0112048 [hep-ph].
 [13] X.-G. He and G.-L. Lin, *Phys. Lett. B* **454**, 123 (1999).
 [14] E. Kou, *Phys. Rev. D* **63**, 054027 (2001).
 [15] S. Dubey, *Search for the decay $B_s^0 \rightarrow \eta' X_{s\bar{s}}$ Using a Semi-Inclusive Method at the Belle Experiment*, Ph.D. thesis, University of Hawaii at Manoa (2020), unpublished.
 [16] T. Abe *et al.*, *Prog. Theor. Exp. Phys.* **2013**, 03A001 (2013).
 [17] A. Datta (University of Mississippi), private communication (2020).
 [18] J. Brodzicka *et al.*, *Prog. Theor. Exp. Phys.* **2012**, 04D001 (2012).
 [19] S. Esen *et al.* (Belle Collaboration), *Phys. Rev. D* **87**, 031101 (2013).
 [20] D. J. Lange, *Nucl. Instrum. and Meth. A* **462**, 152 (2001).
 [21] R. Brun *et al.*, GEANT 3.21, CERN Report DD/EE/84-1 (1984).
 [22] E. Barberio, B. van Eijk, and Z. Was, *Comp. Phys. Commun.* **66**, 115 (1991).
 [23] T. Sjostrand, S. Mrenna, and P. Skands, *JHEP* **2006** (2006), 026.
 [24] H. Hirano *et al.*, *Nucl. Instrum. and Meth. A* **455**, 294 (2000).
 [25] T. Iijima *et al.*, *Nucl. Instrum. and Meth. A* **453**, 321 (2000).
 [26] H. Kichimi *et al.*, *Nucl. Instrum. and Meth. A* **453**, 315 (2000).
 [27] P. Zyla *et al.* (Particle Data Group), *Prog. Theor. Exp. Phys.* **2020**, 083C01 (2020).
 [28] G. C. Fox and S. Wolfram, *Phys. Rev. Lett.* **41**, 1581 (1978).
 [29] M. Feindt and U. Kerzel, *Nucl. Instrum. and Meth. A* **559**, 190 (2006).
 [30] S. H. Lee *et al.* (Belle Collaboration), *Phys. Rev. Lett.* **91**, 261801 (2003).
 [31] H. Albrecht *et al.* (ARGUS Collaboration), *Phys. Lett. B* **241**, 278 (1990).
 [32] The number of unreconstructed modes is discussed in the supplementary material.
 [33] A discussion of the uncertainties is given in the accompanying supplementary material.
 [34] Estimates of the FM uncertainty are given in the supplementary material.
 [35] R. Aaij *et al.* (LHCb Collaboration), *JHEP* **1705**, 158 (2017).